THE JOURNAL OF PHYSICAL CHEMISTRY A

Article

pubs.acs.org/JPCA

Interaction of Metal Ions with the His13-His14 Sequence Relevant to Alzheimer's Disease

Xiangtao Kong,[†] Zhi Zhao,[†,‡] Xin Lei,[†] Bingbing Zhang,[†,§] Dongxu Dai,[†] and Ling Jiang*[,†]

[†]State Key Laboratory of Molecular Reaction Dynamics, iChEM, Dalian Institute of Chemical Physics, Chinese Academy of Sciences, Dalian 116023, Liaoning, China

[‡]School of Physics and Optoelectronic Technology, Dalian University of Technology, Dalian 116024, China

[§]State Key Laboratory of Fine Chemicals, Dalian University of Technology, Dalian 116024, China

Supporting Information

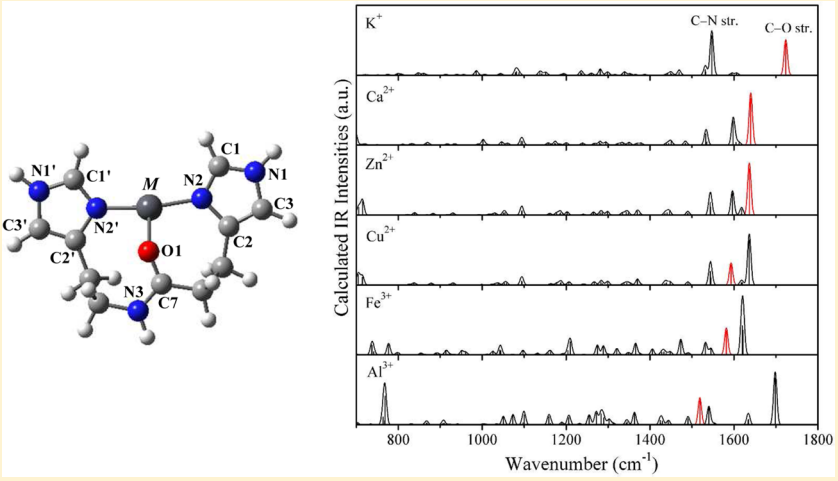

ABSTRACT: The interaction of a series of metal ions (i.e., groups 1 and 2, first-row transition metals, and groups 11−14) with the His13-His14 sequence relevant to Alzheimer's disease has been studied using quantum chemical calculations. Metal ions prefer to occupy three coordination sites at two N_δ of the imidazole rings and one carbonyl oxygen. Simulated IR spectra reveal that vibrational frequency of C−O stretch affords a sensitive probe for understanding the interaction of His13-His14 with metal ions. The relative strength of the interaction of His13-His14 with the representative metal ions follows the order of $K^+ < Ca^{2+} < Zn^{2+} < Cu^{2+} < Fe^{3+} < Al^{3+}$, which is closely correlated with the available experimental results, providing a vivid physical picture about how metal ions bind to amyloid β-peptide. IR spectra of the $[M\cdot(\text{His13-His14})]^{n+}$ complexes could be measured by infrared photodissociation spectroscopic technique and thus afford useful information for the understanding of structure−function relationship and the design of suitable drugs.

1. INTRODUCTION

Alzheimer's disease (AD) is a most common neurodegenerative disease among the aged.[1] The patients suffer from progressive loss of memory and thinking ability. It is now widely accepted that an aggregated form of the amyloid β-peptide (Aβ) is the major component of senile plaques that are diagnostic of AD.[2−10] In vitro studies exhibit that post-mortem brain tissues of AD patients have transition metals with high concentrations, such as Zn^{2+}, Cu^{2+}, and Fe^{3+}, which generally promote Aβ aggregation.[11−15] The interaction of redox active metal ions (i.e., Fe^{3+} and Cu^{2+}) with Aβ might also lead to the formation of reactive oxygen species, which typifies AD neuropathology and precedes Aβ deposition in AD.[8,16−18] In particular, the roles of zinc and copper in AD have been investigated in great detail by nuclear magnetic resonance (NMR),[19−23] electron paramagnetic resonance (EPR),[19,24] X-ray absorption spectroscopy,[25,26] Fourier transform infrared spectroscopy,[7,27] theoretical modeling,[9,28−31] and so on.

NMR and EPR experimental results have shown that the coordination of Cu^{2+} and Zn^{2+} to monomeric Aβ is tetravalent in both aqueous solution and lipid environments, in which the His6, His13, and His14 residues are involved.[19] The oxygen ligand of Ala2 in the Cu^{2+}-Aβ(1−16) system has been identified via continuous wave electron paramagnetic resonance spectroscopy and hyperfine sublevel correlation.[24] The binding sites of Cu^{2+} on the amyloid fibrils of full-length Aβ(1−40) have been explored by ^{13}C solid-state NMR, revealing that the Cu^{2+} ion is coordinated to the N atoms of His residues and O atoms

Received: February 11, 2015
Revised: March 18, 2015
Published: March 23, 2015

DOI: 10.1021/acs.jpca.5b01443
J. Phys. Chem. A 2015, 119, 3528−3534

in Val-40 as well as in Glu side chains (Glu3, Glu11, and/or Glu22).[23] For the interactions of Zn^{2+} between monomeric Aβ, it is most likely that the coordination site of Zn(Aβ) is made of 4 to 6 ligands, including His6, His13, and His14.[7]

Recent classical molecular dynamics (MD) simulations and replica exchange MD simulations of the Zn^{2+}-Aβ_{42} complex have demonstrated that the solvation energy for large Zn^{2+}-Aβ_{42} oligomers is remarkably decreased upon the coordination of zinc ion, resulting in the promotion of their aggregation.[28] The interaction between iron ion and β-amyloid peptide has been investigated by ab initio computational methodology, in which the His13-His14 sequence was modeled by *N*-(2-(1H-imidazol-4-yl)ethyl)-3-(1H-imidazol-4-yl) propanamide, His6 by imidazole, and Tyr10 by phenol. It has been found that Fe^{3+} is coordinated to tyrosine, but its coordination to imidazoles cannot be ruled out.[29] Homology modeling approach has been combined with quantum mechanics to derive plausible three-dimensional models for Cu^{2+}-Aβ(1−16) with three histidines in their coordination sphere, indicating that the Cu^{2+} ion coordinates to His6, His13, His14, and Ala2.[30] Systematically, there is little molecular understanding of the interaction of monomeric amyloid β-peptide with a series of metal ions covering both main group and transition metal ions.

Infrared photodissociation (IRPD) spectroscopy of mass-selected complexes has emerged as a powerful tool for the structural characterization of the gas-phase complexes relevant to biological chemistry.[32−40] Under readily achievable experimental conditions, absorption of single IR photon or multiple IR photons by a cluster can induce a measurable increase in the sequence, resulting in IRPD spectra that closely resemble linear absorption spectra. Compared with the conventional vibrational spectroscopy, IRPD has advantages of high selectivity, high sensitivity, and being a background-free consequence technique.

Stimulated by the studies on the chemistry of Alzheimer's disease, herein, we present a study on the interaction of a series of metal ions with monomeric amyloid β-peptide via a cluster model. Simulated results of the $[M\cdot(\text{His13-His14})]^{n+}$ complexes reveal that the C−O stretching vibrational frequencies afford a sensitive probe for exploring these interactions. The relative strength of the interaction of His13-His14 with the representative metal ions follows the order of $K^+ < Ca^{2+} < Zn^{2+} < Cu^{2+} < Fe^{3+} < Al^{3+}$. Overall correlation of this order with the available experimental results has been obtained.

2. THEORETICAL METHODS

Quantum chemical calculations are carried out using the TURBOMOLE V6.3.1 program suite.[41] Initial configurations are built on the basis of the relevant structures reported in the literature. Considering that the interaction of the organic complexes with metal ions could be properly predicted by the BHLYP density functional as compared to the highly correlated CCSD(T) method,[30,42] all the present calculations employ the BHLYP method. The DZP basis set is used for C, H, O, N atoms, and def2-TZVP basis set for all the metal atoms together with an effective core potential for the fifth-row and sixth-row elements. Metal ions with the interested valence states are considered with respect to their existence in human bodies. For metal ions with open shell, different spin multiplicities are studied. The geometries are fully optimized without any restrictions. Harmonic vibrational frequencies are calculated at the same level. All reported structures are true minima without imaginary vibrational frequencies. Harmonic vibrational frequencies are scaled by a factor of 0.95,[42] and IR stick spectra are convoluted by a Gaussian line shape function with a width of 10 cm^{-1} (fwhm).

Since the His13-His14 sequence is the important ligand in Aβ that capture metal ions,[5−9,19,23,24,28−31] the effect of metal coordination on Aβ is explored via the $[M\cdot(\text{His13-His14})]^{n+}$ complexes, in which the His13-His14 sequence is modeled by N-(2-(1H-imidazol-4-yl)ethyl)-3-(1H-imidazol-4-yl)-propanamide.[29,31] Both main group and transition metal ions are considered here.

3. RESULTS

The optimized structures of the $[M\cdot(\text{His13-His14})]^{n+}$ complexes (M^{n+} = group 1, group 2, first-row transition metals, and groups 11−14 metals) are presented in Figure 1, in which the

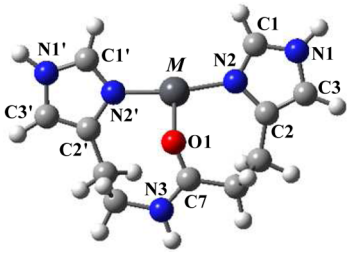

Figure 1. Optimized structure of the $[M\cdot(\text{His13-His14})]^{n+}$ complexes (N, blue; C, gray; H, light gray; O, red; metal ions, black).

atoms are labeled for the convenience of discussion. All the metal ions bind to the His13-His14 complex in a tridentate fashion, occupying three coordination sites at two N_δ of the imidazole rings and one carbonyl oxygen, which is consistent with the previous studies on the interaction of β-amyloid peptide with copper and iron ions.[29,31]

Simulated IR spectra of the $[M\cdot(\text{His13-His14})]^+$ complexes (M^+ = Li^+, Na^+, K^+, Rb^+, and Cs^+) are representatively shown in Figure 2, and those for the remaining metal ions are illustrated in Figures S1−S6 of the Supporting Information. It can be seen from Figure 2 that three groups of intense bands are observed around 1550, 1720, and 3570 cm^{-1}, respectively, which are

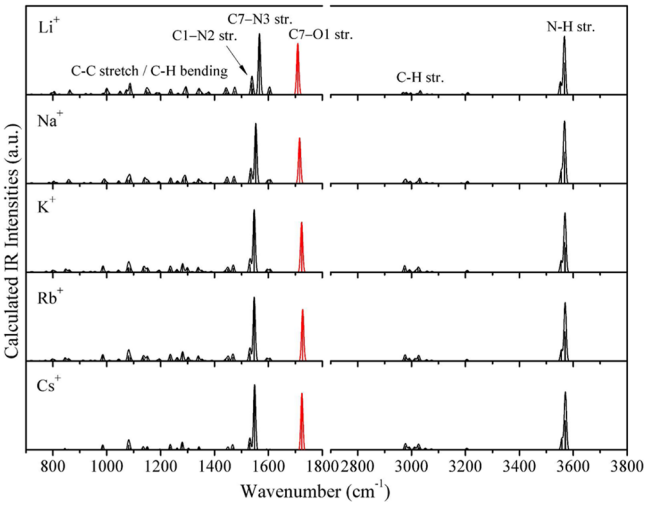

Figure 2. Simulated IR spectra of the $[M\cdot(\text{His13-His14})]^+$ complexes (M^+ = Li^+, Na^+, K^+, Rb^+, and Cs^+). The C7−O1 stretch is depicted in red.

DOI: 10.1021/acs.jpca.5b01443
J. Phys. Chem. A 2015, 119, 3528−3534

assigned to the C7−N3, C7−O1, and N−H (N1−H or N1′-H) stretches. In contrast, the C1−N2 (or C1′-N2′) stretching in the imidazole ring, C−C stretching, C−H stretching, and C−H bending modes weakly appear in the IR spectra. For the Li^+, Na^+, K^+, Rb+, and Cs^+ ions, vibrational frequency of the C7−N3 stretch is calculated to be 1567, 1553, 1547, 1547, and 1549 cm^{-1}, the C7−O1 stretch to be 1709, 1716, 1723, 1727, and 1724 cm^{-1}, and the N−H stretch to be 3567, 3567, 3569, 3569, and 3570 cm^{-1}, respectively. Considering that the metal ions directly interact with the His13-His14 complex in the O1 position, the C7−O1 stretching vibrational frequencies are expected to be more sensitive than those of C7−N3 and N1−H (or N1′-H) stretches for the reflection of the effect of metal coordination, which is affirmed by the comparison among the K^+, Ca^{2+}, Zn^{2+}, Cu^{2+}, Fe^{3+}, and Al^{3+} ions (vide infra). Accordingly, the C−O stretching vibrational frequencies in the $[M\cdot(\text{His13-His14})]^{n+}$ complexes and their deviations from bare His13-His14 are summarized in Table 1.

In Figure S1 of the Supporting Information, the C7−O1 mode is predicted at 1587, 1650, 1641, 1640, and 1633 cm^{-1} for Be^{2+}, Mg^{2+}, Ca^{2+}, Sr^{2+}, and Ba^{2+}, respectively. As compared with the C7−O1 stretching vibrational frequency in the free His13-His14 sequence, Be^{2+} causes the largest red-shift of ν_{C-O} by 171 cm^{-1}, while Mg^{2+} results in a smallest red-shift of ν_{C-O} by 108 cm^{-1} among the group 2 metal ions (Table 1). However, the IR intensity of the C7−O1 stretch is much reduced by Be^{2+} as compared to other alkaline-earth metal ions. From Mg^{2+} to Ba^{2+}, the deviation $\Delta\nu_{C-O}$ monotonically increases from 108 to 125 cm^{-1}.

Table 1. C−O Stretching Vibrational Frequencies (ν_{C-O}) in the $[M\cdot(\text{His13-His14})]^{n+}$ Complexes, Their Deviations ($\Delta\nu_{C-O}$) from Bare His13-His14 (Negative Values Denote Red-Shift), and C−O Bond Lengths (R_{C-O})

species	ν_{C-O} (cm^{-1})	$\Delta\nu_{C-O}$ (cm^{-1})	R_{C-O} (Å)
His13-His14	1758	0	1.213
$[Li\cdot(\text{His13-His14})]^+$	1709	−49	1.227
$[Na\cdot(\text{His13-His14})]^+$	1716	−42	1.224
$[K\cdot(\text{His13-His14})]^+$	1723	−35	1.221
$[Rb\cdot(\text{His13-His14})]^+$	1727	−31	1.220
$[Cs\cdot(\text{His13-His14})]^+$	1724	−34	1.221
$[Be\cdot(\text{His13-His14})]^{2+}$	1587	−171	1.266
$[Mg\cdot(\text{His13-His14})]^{2+}$	1650	−108	1.253
$[Ca\cdot(\text{His13-His14})]^{2+}$	1641	−117	1.251
$[Sr\cdot(\text{His13-His14})]^{2+}$	1640	−118	1.249
$[Ba\cdot(\text{His13-His14})]^{2+}$	1633	−125	1.249
$[Sc\cdot(\text{His13-His14})]^{3+}$	1498	−260	1.299
$[Ti\cdot(\text{His13-His14})]^{4+}$	1188	−570	1.354
$[V\cdot(\text{His13-His14})]^{4+}$	1262	−496	1.309
$[Cr\cdot(\text{His13-His14})]^{3+}$	1589	−169	1.261
$[Mn\cdot(\text{His13-His14})]^{2+}$	1598	−160	1.253
$[Fe\cdot(\text{His13-His14})]^{3+}$	1582	−176	1.261
$[Fe\cdot\text{His13-His14})]^{2+}$	1591	−167	1.257
$[Co\cdot(\text{His13-His14})]^{3+}$	1591	−167	1.260
$[Ni\cdot(\text{His13-His14})]^{2+}$	1594	−164	1.256
$[Cu\cdot(\text{His13-His14})]^{2+}$	1593	−165	1.256
$[Cu\cdot(\text{His13-His14})]^+$	1711	−47	1.222
$[Ag\cdot(\text{His13-His14})]^+$	1721	−37	1.219
$[Au\cdot(\text{His13-His14})]^+$	1763	+5	1.209
$[Zn\cdot(\text{His13-His14})]^{2+}$	1637	−121	1.254
$[Cd\cdot(\text{His13-His14})]^{2+}$	1641	−117	1.246
$[Hg\cdot(\text{His13-His14})]^{2+}$	1655	−103	1.238
$[Al\cdot(\text{His13-His14})]^{3+}$	1519	−239	1.293
$[Ga\cdot(\text{His13-His14})]^{3+}$	1515	−243	1.291
$[In\cdot(\text{His13-His14})]^{3+}$	1549	−209	1.280
$[Tl\cdot(\text{His13-His14})]^{3+}$	1555	−203	1.271
$[Si\cdot(\text{His13-His14})]^{4+}$	1442	−316	1.346
$[Ge\cdot(\text{His13-His14})]^{4+}$	1447	−311	1.340
$[Sn\cdot(\text{His13-His14})]^{4+}$	1460	−298	1.322
$[Pb\cdot(\text{His13-His14})]^{2+}$	1588	−170	1.257

IR spectra of the His13-His14 sequence coordinated with the first-row transition metal ions are depicted in Figure S2 of the Supporting Information. The ν_{C-O} value is simulated to be 1498, 1188, 1262, 1589, 1598, 1582, 1591, 1591, 1594, and 1593 cm^{-1} for Sc^{3+}, Ti^{4+}, V^{4+}, Cr^{3+}, Mn^{2+}, Fe^{3+}, Fe^{2+}, Co^{3+}, Ni^{2+}, and Cu^{2+}, respectively. As listed in Table 1, the coordination of the Sc^{3+}, Ti^{4+}, and V^{4+} ions with the His13-His14 complex leads to significant deviations of C−O stretch ($\Delta\nu_{C-O}$ = −260 ∼ −570 cm^{-1}), while the Cr^{3+}, Mn^{2+}, Fe^{3+}, Fe^{2+}, Co^{3+}, Ni^{2+}, and Cu^{2+} ions yield the $\Delta\nu_{C-O}$ values of −160 ∼ −176 cm^{-1}. In contrast, the monovalent Cu^+ and Ag^+ ions exhibit relatively smaller $\Delta\nu_{C-O}$ values similar to the alkali metal ions, while the Au^+ ion results in a slight blue-shift of C7−O1 stretches with respect to the bare His13-His14 sequence (Figure S3 of the Supporting Information and Table 1). C7−O1 stretching mode appears at 1637, 1641, and 1655 cm^{-1} for Zn^{2+}, Cd^{2+}, and Hg^{2+} (Figure S4 of the Supporting Information and Table 1), respectively, in which the $\Delta\nu_{C-O}$ value ranges from −121 to −103 cm^{-1}.

In Figure S5 of the Supporting Information, the peak of the C7−O1 stretch presents around 1519, 1515, 1549, and 1555 cm^{-1} for Al^{3+}, Ga^{3+}, In^{3+}, and Tl^{3+}, respectively. The Al^{3+} and Ga^{3+} ions give the $\Delta\nu_{C-O}$ values about −240 cm^{-1} (Table 1), whereas the In^{3+} and Tl^{3+} ions yield slightly smaller $\Delta\nu_{C-O}$ values of −209 and −203 cm^{-1}, respectively. In addition, the N−H out-of-plane bend motions (γ_{N-H}) are observed around 760 cm^{-1}. It can be seen from Figure S6 of the Supporting Information that the C7−O1 stretch is calculated at 1442, 1447, 1460, and 1588 cm^{-1} for Si^{4+}, Ge^{4+}, Sn^{4+}, and Pb^{2+}, respectively, providing the $\Delta\nu_{C-O}$ values from −316 to −170 cm^{-1}.

4. DISCUSSION

On the basis of the abundance and importance of metal ions in the human body, the representative K^+, Ca^{2+}, Zn^{2+}, Cu^{2+}, Fe^{3+}, and Al^{3+} ions are selected to derive the general trend of the relative strength for the interaction in-between metal ions and the His13-His14 sequence in Aβ. NBO partial charges of C1 and O1 atoms, Wiberg bond orders of the CO moiety, C−O bond lengths, C−O stretching vibrational frequencies in the $[M\cdot(\text{His13-His14})]^{n+}$ complexes (M^{n+} = K^+, Ca^{2+}, Zn^{2+}, Cu^{2+}, Fe^{3+}, and Al^{3+}), and their shifts with respect to free His13-His14 are summarized in Table 2. IR spectra of these $[M\cdot(\text{His13-His14})]^{n+}$ complexes in the 800−1800 cm^{-1} region are compared in Figure 3. Since metal cations are bound not only to the CO moiety but also to N sites, the Wiberg bond order of CO should be more reliable for assessing the effect of metal cation on CO frequency red-shift than binding energy of metal cation with His13-His14. Accordingly, red-shifts of C−O stretching vibrational frequencies as a function of Wiberg bond orders of the CO moiety are depicted in Figure 4.

It can be seen from the aforementioned results that metal ions directly bind to the oxygen terminal of the C7−O1 sites, and the C7−O1 stretching vibrational frequencies readily differ

DOI: 10.1021/acs.jpca.5b01443
J. Phys. Chem. A 2015, 119, 3528−3534

Table 2. NBO Partial Charges of C1 and O1 Atoms (q_C and q_O), Wiberg Bond Orders of the CO Moiety (P_{C-O}), C−O Bond Lengths (R_{C-O}), C−O Stretching Vibrational Frequencies (ν_{C-O}) in the $[M\cdot(His13\text{-}His14)]^{n+}$ Complexes (M^{n+} = K^+, Ca^{2+}, Zn^{2+}, Cu^{2+}, Fe^{3+}, and Al^{3+}), and Their Shifts ($\Delta\nu_{C-O}$) with Respect to Bare His13-His14 (Negative Values Denote Red-Shift)

species	q_C	q_O	P_{C-O}	R_{C-O} (Å)	ν_{C-O} (cm^{-1})	$\Delta\nu_{C-O}$ (cm^{-1})
His13-His14	0.80	−0.72	1.60	1.213	1758	–
$[K\cdot(His13\text{-}His14)]^+$	0.83	−0.78	1.52	1.221	1723	−35
$[Ca\cdot(His13\text{-}His14)]^{2+}$	0.86	−0.90	1.30	1.251	1641	−117
$[Zn\cdot(His13\text{-}His14)]^{2+}$	0.85	−0.87	1.30	1.254	1637	−121
$[Cu\cdot(His13\text{-}His14)]^{2+}$	0.85	−0.82	1.28	1.256	1593	−165
$[Fe\cdot(His13\text{-}His14)]^{3+}$	0.87	−0.87	1.24	1.261	1582	−176
$[Al\cdot(His13\text{-}His14)]^{3+}$	0.86	−0.97	1.07	1.293	1519	−239

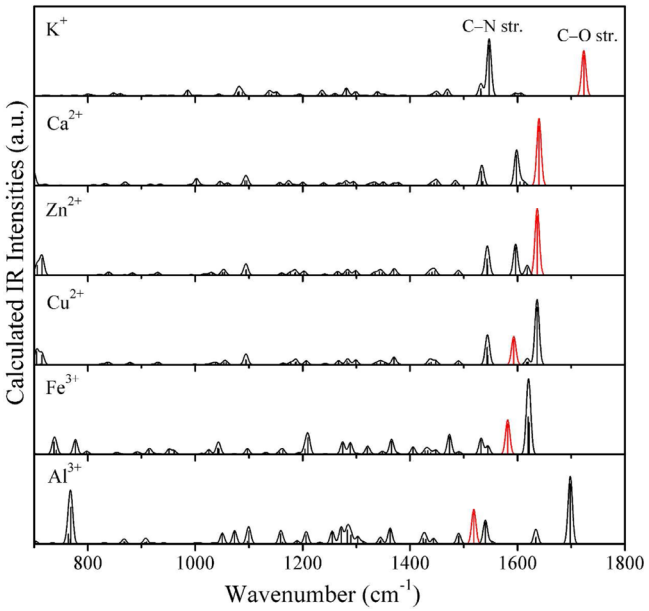

Figure 3. Simulated IR spectra of the $[M\cdot(His13\text{-}His14)]^{n+}$ complexes (M^{n+} = K^+, Ca^{2+}, Zn^{2+}, Cu^{2+}, Fe^{3+}, and Al^{3+}). The C7−O1 stretch is depicted in red.

among various metal ions. To understand the shifts of C7−O1 stretching vibrational frequencies, the effect of metal coordination on the His13-His14 sequence needs to be examined. Positively charged metal carbonyl complexes, $M(CO)_n^+$, have been termed "nonclassical carbonyls".[43−47] Previous studies have demonstrated that a positive charge attached at the carbon atom attracts electronic charge from the oxygen atom toward carbon the end, which leads to less polarized σ- and π-bonds and a more covalent C−O bond. The approach of a metal cation to the oxygen atom (i.e., M^{n+}---OC) has the opposite effect, namely, more polarized σ- and π-bonds and a less covalent C−O bond.[48−51] Such charge polarization has also been observed in the present $[M\cdot(His13\text{-}His14)]^{n+}$ complexes. For instance, the partial charge of C1 and O1 atoms in $[K\cdot(His13\text{-}His14)]^+$ is 0.83 e and −0.78 e (Table 2), respectively, becoming more positive for the C atom and more negative for

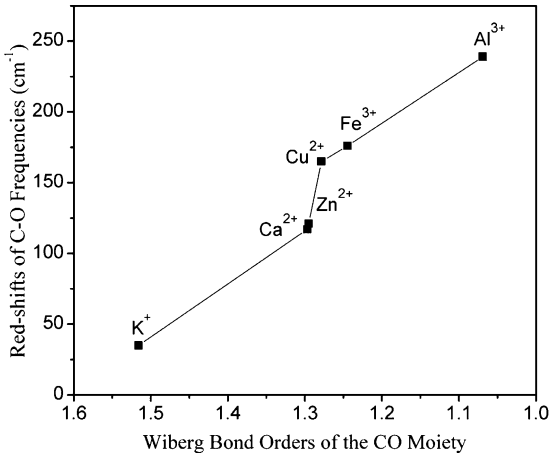

Figure 4. Red-shifts of C−O stretching vibrational frequencies as a function of Wiberg bond orders of the CO moiety in the $[M\cdot(His13\text{-}His14)]^{n+}$ complexes (M^{n+} = K^+, Ca^{2+}, Zn^{2+}, Cu^{2+}, Fe^{3+}, and Al^{3+}).

the O atom than that in the bare His13-His14. Similar alternation for electronic charges of C and O atoms by the coordination of metal cation has also been found for Ca^{2+}, Zn^{2+}, Cu^{2+}, Fe^{3+}, and Al^{3+} (Table 2), respectively. Wiberg bond order of the CO moiety in the $[M\cdot(His13\text{-}His14)]^{n+}$ complex is predicted to be 1.52, 1.30, 1.30, 1.28, 1.24, and 1.07 for K^+, Ca^{2+}, Zn^{2+}, Cu^{2+}, Fe^{3+}, and Al^{3+} (Table 2), respectively, which is smaller than that in the bare His13-His14, leading to longer C−O bond distance. Consequently, the activation of the C−O bond by metal cations follows the order of $K^+ < Ca^{2+} < Zn^{2+} < Cu^{2+} < Fe^{3+} < Al^{3+}$, resulting in the increase of red shift of CO stretching vibrational frequencies (Figure 4). Binding energy of metal cation with His13-His14 is calculated to be 55.86, 212.43, 340.85, 353.69, 676.58, and 719.49 kcal/mol for K^+, Ca^{2+}, Zn^{2+}, Cu^{2+}, Fe^{3+}, and Al^{3+}, respectively, implying that the relative strength for its interaction with His13-His14 follows the order of $K^+ < Ca^{2+} < Zn^{2+} < Cu^{2+} < Al^{3+} < Fe^{3+}$.

The K^+ ion loosely binds to the His13-His14 part with the distance in between the potassium and oxygen atoms of 2.495 Å (Table S1 of the Supporting Information). Similarly, the carbonyl oxygen atoms in the GYG signature sequence are held open by structural constraints to coordinate the K^+ ions (~3 Å).[52] The absolute $\Delta\nu_{C-O}$ value for Ca^{2+} (117 cm^{-1}) is much larger than that for K^+ (35 cm^{-1}), suggesting that the interaction of His13-His14 with Ca^{2+} is much stronger than that with K^+. Interestingly, Ca^{2+}-activated K^+ channels of charybdotoxin analogs could be prepared against voltage-gated Kv1.3 channels, in that the affinity of Ca^{2+} is about 20-fold higher than K^+.[53] Because of its strong coordination, calcium plays an important role in AD and becomes a main cause of neurotoxicity if Ca^{2+} concentration is abnormally high inside mitochondria.[54] Aβ may disrupt Cu−prion−protein-mediated NMDA receptors involved in Ca^{2+} signaling, linking the calcium dyshomeostasis and neurotoxicity observed in AD directly to zinc, copper, and Aβ.[55]

It has been demonstrated that the genetic risk factor in familial AD is correlated with higher serum levels of Zn, Cu, and insulin.[56] Zinc dyshomeostasis is a pathological feature of AD[56−58] and Parkinson's disease,[58] etc. Excess Zn^{2+} will ultimately lead to neuronal necrosis or apoptosis.[56,59] Even with very low concentration of Cu^{2+} beyond 10^{-18} M, it may cause oxidative damage.[60] Cu-Aβ also produces ROS by itself, for instance, peroxide formation and lipid peroxidation initiated

DOI: 10.1021/acs.jpca.5b01443
J. Phys. Chem. A 2015, 119, 3528−3534

by Cu^{2+}-induced dityrosine formation from Tyr-10.[61] In this context, Cu^{2+} may confer toxicity to the Aβ in a concentration-dependent manner.[62,63]

Iron homeostasis is normally governed by a range of proteins such as ferritin and transferrin,[64] which store ~25% of the body's iron, mainly as ferric Fe^{3+}, and have been implicated in neurodegeneration.[65] In terms of toxic mechanism, free Fe^{3+} and Al^{3+} have been found to induce tau protein aggregation.[66] As mentioned above, Al^{3+} causes the largest $\Delta\nu_{C-O}$ value among the representative metal ions shown in Figure 3. This is consistent with the fact that Al^{3+} has substituted bound Fe^{2+}/Fe^{3+}, probably leading to free Fe^{2+}/Fe^{3+} and Fenton toxicity, which would enhance the ROS burden and render the CNS more vulnerable to AD risk factors. The aggregation mechanisms of Al^{3+}−Aβ were found to be distinct from those of Zn^{2+} and Cu^{2+}.[67] Independent investigations have suggested that trivalent Al^{3+} ion is key to the formation of plaques,[68] whereas Zn^{2+} and Cu^{2+} are deposited in them adventitiously,[69] although more studies are needed to support these proposals.

For possible treatment of AD, metal chelators are being rapidly developed.[10,70] Various Cu−Zn chelators are known to effectively inhibit amyloid formation in AD transgenic mice.[71] The chelator PBT2 has displayed particular potency and is currently in phase II studies and used as a lead in the exploration for new commercial AD drugs.[72] Considering that active sites and normal regulatory sites of their metal ions can be stripped by too strong of chelators, appropriate and selective binding should be designed.

Considering that the C−O stretches have been successfully resolved in the IRPD spectra of a series of mass-selected complexes radiated by optical parametric oscillator/optical parametric amplifier (OPO/OPA) table-top laser system or infrared free electron laser (IR-FEL) source,[39,73−76] the predicted C−O stretches in the $[M\cdot(His13\text{-}His14)]^{n+}$ complexes could be readily measured by the IRPD technique and thus afford useful information for the understanding of structure−function relationship and the design of suitable drugs. Various efforts may hopefully help to improve the prospects for the millions of people suffering from this terrible disease.

5. CONCLUSIONS

The coordination of a series of metal ions (i.e., groups 1 and 2, first-row transition metals, and groups 11−14) with the His13-His14 sequence is systematically investigated using quantum chemical calculations to model the interaction of metal ions with amyloid β-peptide. All the metal ions bind to the His13-His14 complex in a tridentate fashion, occupying three coordination sites at two N_δ of the imidazole rings and one carbonyl oxygen. Simulated IR spectra of the $[M\cdot(His13\text{-}His14)]^{n+}$ complexes reveal that the C−O stretching vibrational frequency affords a sensitive probe for exploring these interactions. The relative strength of the interaction of His13-His14 with the representative metal ions follows the order of $K^+ < Ca^{2+} < Zn^{2+} < Cu^{2+} < Fe^{3+} < Al^{3+}$. Satisfied correlation of this order with the available experimental results has been obtained. The combination of IRPD technique and theoretical modeling thus provide a vivid physical picture about how the metal ions bind to amyloid β-peptide.

■ ASSOCIATED CONTENT

Supporting Information

Figures S1−S6: IR spectra of $[M\cdot(His13\text{-}His14)]^{n+}$ (M^{n+} = group 2, first-row transition metals, and groups 11−14 metals). Table S1: Bond distances of C7−O1, M−O and C−N in $[M\cdot(His13\text{-}His14)]^{n+}$. This material is available free of charge via the Internet at http://pubs.acs.org.

■ AUTHOR INFORMATION

Corresponding Author

*E-mail: ljiang@dicp.ac.cn. Tel: +86-411-84379857.

Notes

The authors declare no competing financial interest.

■ ACKNOWLEDGMENTS

This work was supported by the National Natural Science Foundation of China (Grant 21273232 and 21327901), the Ministry of Science and Technology of China (Grant 2011YQ09000505), and the Key Research Programme of the Chinese Academy of Science (Grant No. KGZD-EW-T05). L.J. acknowledges Hundred Talents Program of Chinese Academy of Sciences, startup fund from Dalian Institute of Chemical Physics, and *i*ChEM (Collaborative Innovation Center of Chemistry for Energy and Materials).

■ REFERENCES

(1) Goedert, M.; Spillantini, M. G. A Century of Alzheimer's Disease. *Science* **2006**, *314*, 777−781.
(2) Masters, C. L.; Simms, G.; Weinman, N. A.; Multhaup, G.; McDonald, B. L.; Beyreuther, K. Amyloid Plaque Core Protein in Alzheimer Disease and Down Syndrome. *Proc. Natl. Acad. Sci. U.S.A.* **1985**, *82*, 4245−4249.
(3) Hardy, J.; Selkoe, D. J. Medicine: The Amyloid Hypothesis of Alzheimer's Disease: Progress and Problems on the Road to Therapeutics. *Science* **2002**, *297*, 353−356.
(4) Mattson, M. P. Pathways Towards and Away from Alzheimer's Disease. *Nature* **2004**, *430*, 631−639.
(5) Gaggelli, E.; Kozlowski, H.; Valensin, D.; Valensin, G. Copper Homeostasis and Neurodegenerative Disorders (Alzheimer's, Prion, and Parkinson's Diseases and Amyotrophic Lateral Sclerosis). *Chem. Rev.* **2006**, *106*, 1995−2044.
(6) Rauk, A. Why Is the Amyloid Beta Peptide of Alzheimer's Disease Neurotoxic? *Dalton Trans.* **2008**, 1273−1282.
(7) Faller, P.; Hureau, C. Bioinorganic Chemistry of Copper and Zinc Ions Coordinated to Amyloid-Beta Peptide. *Dalton Trans.* **2009**, 1080−1094.
(8) Rauk, A. The Chemistry of Alzheimer's Disease. *Chem. Soc. Rev.* **2009**, *38*, 2698−2715.
(9) Miller, Y.; Ma, B.; Nussinov, R. Polymorphism in Alzheimer A-Beta Amyloid Organization Reflects Conformational Selection in a Rugged Energy Landscape. *Chem. Rev.* **2010**, *110*, 4820−4838.
(10) Kepp, K. P. Bioinorganic Chemistry of Alzheimer's Disease. *Chem. Rev.* **2012**, *112*, 5193−5239.
(11) Mantyh, P. W.; Ghilardi, J. R.; Rogers, S.; Demaster, E.; Allen, C. J.; Stimson, E. R.; Maggio, J. E. Aluminum, Iron, and Zinc Ions Promote Aggregation of Physiological Concentrations of Beta-Amyloid Peptide. *J. Neurochem.* **1993**, *61*, 1171−1174.
(12) Bush, A. I.; Pettingell, W. H.; Multhaup, G.; Paradis, M. D.; Vonsattel, J. P.; Gusella, J. F.; Beyreuther, K.; Masters, C. L.; Tanzi, R. E. Rapid Induction of Alzheimer A-Beta Amyloid Formation by Zinc. *Science* **1994**, *265*, 1464−1467.
(13) Lovell, M. A.; Robertson, J. D.; Teesdale, W. J.; Campbell, J. L.; Markesbery, W. R. Copper, Iron and Zinc in Alzheimer's Disease Senile Plaques. *J. Neurol. Sci.* **1998**, *158*, 47−52.
(14) Atwood, C. S.; Moir, R. D.; Huang, X. D.; Scarpa, R. C.; Bacarra, N. M. E.; Romano, D. M.; Hartshorn, M. K.; Tanzi, R. E.; Bush, A. I.

DOI: 10.1021/acs.jpca.5b01443
J. Phys. Chem. A 2015, 119, 3528−3534

Dramatic Aggregation of Alzheimer A-Beta by Cu(II) Is Induced by Conditions Representing Physiological Acidosis. *J. Biol. Chem.* **1998**, *273*, 12817−12826.
(15) Hung, Y. H.; Bush, A. I.; Cherny, R. A. Copper in the Brain and Alzheimer's Disease. *J. Biol. Inorg. Chem.* **2010**, *15*, 61−76.
(16) Huang, X. D.; Atwood, C. S.; Hartshorn, M. A.; Multhaup, G.; Goldstein, L. E.; Scarpa, R. C.; Cuajungco, M. P.; Gray, D. N.; Lim, J.; Moir, R. D.; et al. The A-Beta Peptide of Alzheimer's Disease Directly Produces Hydrogen Peroxide through Metal Ion Reduction. *Biochemistry* **1999**, *38*, 7609−7616.
(17) Nunomura, A.; Perry, G.; Aliev, G.; Hirai, K.; Takeda, A.; Balraj, E. K.; Jones, P. K.; Ghanbari, H.; Wataya, T.; Shimohama, S.; et al. Oxidative Damage Is the Earliest Event in Alzheimer Disease. *J. Neuropathol. Exp. Neurol.* **2001**, *60*, 759−767.
(18) Dong, J.; Atwood, C. S.; Anderson, V. E.; Siedlak, S. L.; Smith, M. A.; Perry, G.; Carey, P. R. Metal Binding and Oxidation of Amyloid-Beta within Isolated Senile Plaque Cores: Raman Microscopic Evidence. *Biochemistry* **2003**, *42*, 2768−2773.
(19) Curtain, C. C.; Ali, F.; Volitakis, I.; Cherny, R. A.; Norton, R. S.; Beyreuther, K.; Barrow, C. J.; Masters, C. L.; Bush, A. I.; Barnham, K. J. Alzheimer's Disease Amyloid-Beta Binds Copper and Zinc to Generate an Allosterically Ordered Membrane-Penetrating Structure Containing Superoxide Dismutase-Like Subunits. *J. Biol. Chem.* **2001**, *276*, 20466−20473.
(20) Hou, L.; Zagorski, M. G. NMR Reveals Anomalous Copper(II) Binding to the Amyloid A-Beta Peptide of Alzheimer's Disease. *J. Am. Chem. Soc.* **2006**, *128*, 9260−9261.
(21) Gaggelli, E.; Janicka-Klos, A.; Jankowska, E.; Kozlowski, H.; Migliorini, C.; Molteni, E.; Valensin, D.; Valensin, G.; Wieczerzak, E. NMR Studies of the Zn^{2+} Interactions with Rat and Human Beta-Amyloid (1−28) Peptides in Water-Micelle Environment. *J. Phys. Chem. B* **2008**, *112*, 100−109.
(22) Guilloreau, L.; Damian, L.; Coppel, Y.; Mazarguil, H.; Winterhalter, M.; Faller, P. Structural and Thermodynamical Properties of Cu-II Amyloid-Beta 16/28 Complexes Associated with Alzheimer's Disease. *J. Biol. Inorg. Chem.* **2006**, *11*, 1024−1038.
(23) Parthasarathy, S.; Long, F.; Miller, Y.; Xiao, Y.; McElheny, D.; Thurber, K.; Ma, B.; Nussinov, R.; Ishii, Y. Molecular-Level Examination of Cu^{2+} Binding Structure for Amyloid Fibrils of 40-Residue Alzheimer's Beta by Solid-State NMR Spectroscopy. *J. Am. Chem. Soc.* **2011**, *133*, 3390−3400.
(24) Drew, S. C.; Masters, C. L.; Barnham, K. J. Alanine-2 Carbonyl Is an Oxygen Ligand in Cu^{2+} Coordination of Alzheimer's Disease Amyloid-Beta Peptide - Relevance to N-Terminally Truncated Forms. *J. Am. Chem. Soc.* **2009**, *131*, 1195−1207.
(25) Morante, S. The Role of Metals in Beta-Amyloid Peptide Aggregation: X-Ray Spectroscopy and Numerical Simulations. *Curr. Alzheimer Res.* **2008**, *5*, 508−524.
(26) Faller, P.; Hureau, C. Impact of Metallic Ions in Alzheimer's Disease: Insights from XAS Spectroscopy. *Actual. Chim.* **2011**, 88−90.
(27) El Khoury, Y.; Dorlet, P.; Faller, P.; Hellwig, P. New Insights into the Coordination of Cu(II) by the Amyloid-B (16) Peptide from Fourier Transform IR Spectroscopy and Isotopic Labeling. *J. Phys. Chem. B* **2011**, *115*, 14812−14821.
(28) Miller, Y.; Ma, B.; Nussinov, R. Zinc Ions Promote Alzheimer A-Beta Aggregation via Population Shift of Polymorphic States. *Proc. Natl. Acad. Sci. U.S.A.* **2010**, *107*, 9490−9495.
(29) Ali-Torres, J.; Rodriguez-Santiago, L.; Sodupe, M.; Rauk, A. Structures and Stabilities of $Fe^{2+/3+}$ Complexes Relevant to Alzheimer's Disease: An Ab Initio Study. *J. Phys. Chem. A* **2011**, *115*, 12523−12530.
(30) Ali-Torres, J.; Marechal, J.-D.; Rodriguez-Santiago, L.; Sodupe, M. Three Dimensional Models of Cu^{2+}-A-Beta(1−16) Complexes from Computational Approaches. *J. Am. Chem. Soc.* **2011**, *133*, 15008−15014.
(31) Raffa, D. F.; Gomez-Balderas, R.; Brunelle, P.; Rickard, G. A.; Rauk, A. Ab Initio Model Studies of Copper Binding to Peptides Containing a His-His Sequence: Relevance to the Beta-Amyloid Peptide of Alzheimer's Disease. *J. Biol. Inorg. Chem.* **2005**, *10*, 887−902.
(32) Okumura, M.; Yeh, L. I.; Lee, Y. T. The Vibrational Predissociation Spectroscopy of Hydrogen Cluster Ions. *J. Chem. Phys.* **1985**, *83*, 3705−3706.
(33) Bieske, E. J.; Dopfer, O. High-Resolution Spectroscopy of Cluster Ions. *Chem. Rev.* **2000**, *100*, 3963−3998.
(34) von Helden, G.; van Heijnsbergen, D.; Meijer, G. Resonant Ionization Using IR Light: A New Tool to Study the Spectroscopy and Dynamics of Gas-Phase Molecules and Clusters. *J. Phys. Chem. A* **2003**, *107*, 1671−1688.
(35) Lisy, J. M. Infrared Studies of Ionic Clusters: The Influence of Yuan T. Lee. *J. Chem. Phys.* **2006**, *125*, 132302-1−132302-19.
(36) Rizzo, T. R.; Stearns, J. A.; Boyarkin, O. V. Spectroscopic Studies of Cold, Gas-Phase Biomolecular Ions. *Int. Rev. Phys. Chem.* **2009**, *28*, 481−515.
(37) Polfer, N. C.; Oomens, J. Vibrational Spectroscopy of Bare and Solvated Ionic Complexes of Biological Relevance. *Mass Spectrom. Rev.* **2009**, *28*, 468−494.
(38) Fridgen, T. D. Infrared Consequence Spectroscopy of Gaseous Protonated and Metal Ion Cationized Complexes. *Mass Spectrom. Rev.* **2009**, *28*, 586−607.
(39) Garand, E.; Kamrath, M. Z.; Jordan, P. A.; Wolk, A. B.; Leavitt, C. M.; McCoy, A. B.; Miller, S. J.; Johnson, M. A. Determination of Noncovalent Docking by Infrared Spectroscopy of Cold Gas-Phase Complexes. *Science* **2012**, *335*, 694−698.
(40) Wolk, A. B.; Leavitt, C. M.; Garand, E.; Johnson, M. A. Cryogenic Ion Chemistry and Spectroscopy. *Acc. Chem. Res.* **2014**, *47*, 202−210.
(41) *TURBOMOLE*, V6.3 2011; University of Karlsruhe and Forschungszentrum Karlsruhe GmbH: Karlsruhe, Germany, 2011.
(42) Savoca, M.; Wende, T.; Jiang, L.; Langer, J.; Meijer, G.; Dopfer, O.; Asmis, K. R. Infrared Spectra and Structures of Silver-PAH Cation Complexes. *J. Phys. Chem. Lett.* **2011**, *2*, 2052−2056.
(43) Hurlburt, P. K.; Anderson, O. P.; Strauss, S. H. $Ag(CO)B(OTeF_5)_4$: The 1ST Isolable Silver Carbonyl. *J. Am. Chem. Soc.* **1991**, *113*, 6277−6278.
(44) Hurlburt, P. K.; Rack, J. J.; Luck, J. S.; Dec, S. F.; Webb, J. D.; Anderson, O. P.; Strauss, S. H. Nonclassical Metal-Carbonyls: $Ag(CO)^+$ and $Ag(CO)_2^+$. *J. Am. Chem. Soc.* **1994**, *116*, 10003−10014.
(45) Rack, J. J.; Webb, J. D.; Strauss, S. H. $Cu(CO)_n^+$ Complex Ions in the Solid State (n = 1, 2, 3). *Inorg. Chem.* **1996**, *35*, 277−278.
(46) Lupinetti, A. J.; Frenking, G.; Strauss, S. H. Nonclassical Metal Carbonyls: Appropriate Definitions with a Theoretical Justification. *Angew. Chem., Int. Ed.* **1998**, *37*, 2113−2116.
(47) Velasquez, J., III; Njegic, B.; Gordon, M. S.; Duncan, M. A. IR Photodissociation Spectroscopy and Theory of $Au^+(CO)_n$ Complexes: Nonclassical Carbonyls in the Gas Phase. *J. Phys. Chem. A* **2008**, *112*, 1907−1913.
(48) Goldman, A. S.; KroghJespersen, K. Why Do Cationic Carbon Monoxide Complexes Have High C-O Stretching Force Constants and Short C-O Bonds? Electrostatic Effects, Not Sigma-Bonding. *J. Am. Chem. Soc.* **1996**, *118*, 12159−12166.
(49) Lupinetti, A. J.; Fau, S.; Frenking, G.; Strauss, S. H. Theoretical Analysis of the Bonding between CO and Positively Charged Atoms. *J. Phys. Chem. A* **1997**, *101*, 9551−9559.
(50) Frenking, G.; Loschen, C.; Krapp, A.; Fau, S.; Strauss, S. H. Electronic Structure of CO: An Exercise in Modern Chemical Bonding Theory. *J. Comput. Chem.* **2007**, *28*, 117−126.
(51) Chen, M.; Zhang, Q.; Zhou, M.; Andrada, D. M.; Frenking, G. Carbon Monoxide Bonding With BeO and $BeCO_3$: Surprisingly High CO Stretching Frequency of $OCBeCO_3$. *Angew. Chem., Int. Ed.* **2015**, *54*, 124−128.
(52) Shieh, C. C.; Coghlan, M.; Sullivan, J. P.; Gopalakrishnan, M. Potassium Channels: Molecular Defects, Diseases, and Therapeutic Opportunities. *Pharmacol. Rev.* **2000**, *52*, 557−593.
(53) Rauer, H.; Lanigan, M. D.; Pennington, M. W.; Aiyar, J.; Ghanshani, S.; Cahalan, M. D.; Norton, R. S.; Chandy, K. G. Structure-Guided Transformation of Charybdotoxin Yields an Analog that

DOI: 10.1021/acs.jpca.5b01443
J. Phys. Chem. A 2015, 119, 3528−3534

Selectively Targets Ca^{2+}-Activated over Voltage-Gated K^+ Channels. *J. Biol. Chem.* **2000**, *275*, 1201−1208.
(54) Ankarcrona, M.; Dypbukt, J. M.; Bonfoco, E.; Zhivotovsky, B.; Orrenius, S.; Lipton, S. A.; Nicotera, P. Glutamate-Induce Neuronal Death: A Succession of Necrosis or Apoptosis Depending on Mitochondrial-Function. *Neuron* **1995**, *15*, 961−973.
(55) You, H.; Tsutsui, S.; Hameed, S.; Kannanayakal, T. J.; Chen, L.; Xia, P.; Engbers, J. D. T.; Lipton, S. A.; Stys, P. K.; Zamponi, G. W. A-Beta Neurotoxicity Depends on Interactions between Copper Ions, Prion Protein, and N-Methyl-D-Aspartate Receptors. *Proc. Natl. Acad. Sci. U.S.A.* **2012**, *109*, 1737−1742.
(56) Burnet, F. M. A Possible Role of Zinc in the Pathology of Dementia. *Lancet* **1981**, *1*, 186−188.
(57) Bitanihirwe, B. K. Y.; Cunningham, M. G. Zinc: The Brain's Dark Horse. *Synapse* **2009**, *63*, 1029−1049.
(58) Hozumi, I.; Hasegawa, T.; Honda, A.; Ozawa, K.; Hayashi, Y.; Hashimoto, K.; Yamada, M.; Koumura, A.; Sakurai, T.; Kimura, A.; et al. Patterns of Levels of Biological Metals in CSF Differ among Neurodegenerative Diseases. *J. Neurol. Sci.* **2011**, *303*, 95−99.
(59) Koh, J. Y.; Suh, S. W.; Gwag, B. J.; He, Y. Y.; Hsu, C. Y.; Choi, D. W. The Role of Zinc in Selective Neuronal Death after Transient Global Cerebral Ischemia. *Science* **1996**, *272*, 1013−1016.
(60) Rae, T. D.; Schmidt, P. J.; Pufahl, R. A.; Culotta, V. C.; O'Halloran, T. V. Undetectable Intracellular Free Copper: The Requirement of a Copper Chaperone for Superoxide Dismutase. *Science* **1999**, *284*, 805−808.
(61) Opazo, C.; Huang, X. D.; Cherny, R. A.; Moir, R. D.; Roher, A. E.; White, A. R.; Cappai, R.; Masters, C. L.; Tanzi, R. E.; Inestrosa, N. C.; Bush, A. I. Metalloenzyme-Like Activity of Alzheimer's Disease Beta-Amyloid: Cu-Dependent Catalytic Conversion of Dopamine, Cholesterol, and Biological Reducing Agents to Neurotoxic H_2O_2. *J. Biol. Chem.* **2002**, *277*, 40302−40308.
(62) Sarell, C. J.; Wilkinson, S. R.; Viles, J. H. Substoichiometric Levels of Cu^{2+} Ions Accelerate the Kinetics of Fiber Formation and Promote Cell Toxicity of Amyloid-Beta from Alzheimer Disease. *J. Biol. Chem.* **2010**, *285*, 41533−41540.
(63) Pedersen, J. T.; Ostergaard, J.; Rozlosnik, N.; Gammelgaard, B.; Heegaard, N. H. H. Cu(II) Mediates Kinetically Distinct, Non-Amyloidogenic Aggregation of Amyloid-Beta Peptides. *J. Biol. Chem.* **2011**, *286*, 26952−26963.
(64) Ponka, P.; Beaumont, C.; Richardson, D. R. Function and Regulation of Transferrin and Ferritin. *Semin. Hematol.* **1998**, *35*, 35−54.
(65) Friedman, A.; Arosio, P.; Finazzi, D.; Koziorowski, D.; Galazka-Friedman, J. Ferritin As an Amportant Player in Neurodegeneration. *Parkinsonism & Related Disorders* **2011**, *17*, 423−30.
(66) Bader, B.; Nuebling, G.; Mehle, A.; Nobile, S.; Kretzschmar, H.; Giese, A. Single Particle Analysis of Tau Oligomer Formation Induced by Metal Ions and Organic Solvents. *Biochem. Biophys. Res. Commun.* **2011**, *411*, 190−196.
(67) Chen, W.-T.; Liao, Y.-H.; Yu, H.-M.; Cheng, I. H.; Chen, Y.-R. Distinct Effects of Zn^{2+}, Cu^{2+}, Fe^{3+}, and Al^{3+} on Amyloid-Beta Stability, Oligomerization, and Aggregation. *J. Biol. Chem.* **2011**, *286*, 9646−9656.
(68) House, E.; Collingwood, J.; Khan, A.; Korchazkina, O.; Berthon, G.; Exley, C. Aluminium, Iron, Zinc and Copper Influence the in vitro Formation of Amyloid Fibrils of A-Beta(42) in a Manner Which May Have Consequences for Metal Chelation Therapy in Alzheimer's Disease. *J. Alzheimer's Dis.* **2004**, *6*, 291−301.
(69) Exley, C. Aluminium and Iron, but Neither Copper Nor Zinc, are Key to the Precipitation of Beta-Sheets of A-Beta(42) in Senile Plaque Cores in Alzheimer's Disease. *J. Alzheimer's Dis.* **2006**, *10*, 173−177.
(70) Scott, L. E.; Orvig, C. Medicinal Inorganic Chemistry Approaches to Passivation and Removal of Aberrant Metal Ions in Disease. *Chem. Rev.* **2009**, *109*, 4885−4910.
(71) Cherny, R. A.; Atwood, C. S.; Xilinas, M. E.; Gray, D. N.; Jones, W. D.; McLean, C. A.; Barnham, K. J.; Volitakis, I.; Fraser, F. W.; Kim, Y. S.; et al. Treatment with a Copper-Zinc Chelator Markedly and Rapidly Inhibits Beta-Amyloid Accumulation in Alzheimer's Disease Transgenic Mice. *Neuron* **2001**, *30*, 665−676.
(72) Faux, N. G.; Ritchie, C. W.; Gunn, A.; Rembach, A.; Tsatsanis, A.; Bedo, J.; Harrison, J.; Lannfelt, L.; Blennow, K.; Zetterberg, H.; et al. PBT2 Rapidly Improves Cognition in Alzheimer's Disease: Additional Phase II Analyses. *J. Alzheimer's Dis.* **2010**, *20*, 509−516.
(73) Walker, N. R.; Walters, R. S.; Duncan, M. A. Frontiers in the Infrared Spectroscopy of Gas Phase Metal Ion Complexes. *New J. Chem.* **2005**, *29*, 1495−1503.
(74) Garand, E.; Wende, T.; Goebbert, D. J.; Bergmann, R.; Meijer, G.; Neumark, D. M.; Asmis, K. R. Infrared Spectroscopy of Hydrated Bicarbonate Anion Clusters: $HCO_3^-(H_2O)_{1-10}$. *J. Am. Chem. Soc.* **2010**, *132*, 849−856.
(75) Wende, T.; Wanko, M.; Jiang, L.; Meijer, G.; Asmis, K. R.; Rubio, A. Spectroscopic Characterization of Solvent-Mediated Folding in Dicarboxylate Dianions. *Angew. Chem., Int. Ed.* **2011**, *50*, 3807−3810.
(76) Wang, G.; Chi, C.; Cui, J.; Xing, X.; Zhou, M. Infrared Photodissociation Spectroscopy of Mononuclear Iron Carbonyl Anions. *J. Phys. Chem. A* **2012**, *116*, 2484−2489.

DOI: 10.1021/acs.jpca.5b01443
J. Phys. Chem. A 2015, 119, 3528−3534